



Electrochemical oxidation of organics in sulfate solutions on boron-doped diamond electrode: Multiple pathways for sulfate radical generation



Yong-Uk Shin^{a,b}, Ha-Young Yoo^a, Yong-Yoon Ahn^a, Min Sik Kim^c, Kang Lee^d, Seungho Yu^d, Changha Lee^c, Kangwoo Cho^e, Hyoung-il Kim^f, Jaesang Lee^{a,b,*}

^a Civil, Environmental, and Architectural Engineering, Korea University, Seoul 136-701, Republic of Korea

^b Energy Environmental Policy and Technology, Green School, Korea University-KIST, Seoul 136-701, Republic of Korea

^c Chemical and Biological Engineering, Seoul National University, Seoul 00826, Republic of Korea

^d Radiation Research Division for Industry and Environment, Korea Atomic Energy Research Institute, Jeongup 580-185, Republic of Korea

^e Environmental Science and Engineering, Pohang University of Science and Technology (POSTECH), Pohang 790-784, Republic of Korea

^f Civil and Environmental Engineering, Yonsei University, Seoul 120-749, Republic of Korea

ARTICLE INFO

Keywords:

Anodic oxidation
Boron-doped diamond electrode
Persulfate activation
Sulfate radical
Resistive heating

ABSTRACT

This study scrutinized the roles of sulfate radicals ($\text{SO}_4^{\cdot-}$) and peroxydisulfate (PDS) formed from SO_4^{2-} in electrochemical organic oxidation on a boron-doped diamond (BDD) electrode. The substrate-specific performance of electrochemical oxidation using SO_4^{2-} as the electrolyte aligned with the reactivity of $\text{SO}_4^{\cdot-}$ produced via radiolysis- or heat-induced PDS activation, but was distinct from the non-selective oxidation efficiency observed in an aqueous ClO_4^- solution. A comparison of the treatment efficiencies using different electrolytes (i.e., Cl^- , SO_4^{2-} , and ClO_4^-) showed no pronounced enhancing effect of $\text{SO}_4^{\cdot-}$ on the anodic oxidation of diverse organics (except perfluoroctanoate), which implied that direct electron transfer and hydroxyl radical-induced oxidation proceeded as complementary reaction routes. Repeated electrolytic oxidation caused substantial electrolyte exchange from Cl^- to ClO_4^- , which retarded organic oxidation accompanied by ClO_4^- accumulation. Conversely, high-yield PDS production observed when SO_4^{2-} was used instead barely reduced treatment efficiency. Together with $\text{SO}_4^{\cdot-}$ detection in the electron paramagnetic resonance spectrum, a correlation between 4-chlorophenol oxidation rate and the faradaic efficiency for SO_4^{2-} formation, monitored in PDS solutions while varying the cathode material, suggested cathodic PDS activation. The electrocatalytic performance was demonstrated to be further improved with anodically formed PDS activation through naturally occurring resistive heating or combination with UV photolysis as a post-treatment step.

1. Introduction

Chemical oxidation utilizing reactive oxidizing species (generated as intermediates from relatively stable precursors) has been recognized as an appealing treatment option, on account of its capability for rapid transformation of pollutants into non-hazardous or low-toxicity products [1,2]. Among the feasible water treatment approaches based on highly reactive oxidants (e.g., Fenton oxidation [3], O_3 or H_2O_2 photolysis [4], and photocatalysis [5–7]), electrochemical oxidation has drawn sustained attention over the past decades due to the following technical benefits: (i) treatability of biologically refractory organics under mild conditions, (ii) environmental compatibility associated with minimal requirement of chemical additives, (iii) ease of operation and maintenance, and (iv) integrability to renewable energy sources [8,9].

Electrochemical water treatment largely rests on anodic oxidation: direct oxidation (i.e., direct electron transfer) on the anode, and indirect oxidation mediated by anodically formed reactive intermediates (e.g., hydroxyl radical ($\cdot\text{OH}$) and reactive chlorine species (RCS)) [8,10,11].

Aside from chemical stability under electrolysis conditions, electrocatalytic behavior for the O_2 evolution reaction has been adopted as a key selection criterion when searching for anodic materials applicable to electrochemical water treatment [10]. Due to their low O_2 evolution overpotential, thin films of RuO_2 and IrO_2 (or a binary mixture) favor substrate-specific oxidation of organics into biodegradable products (i.e., electrochemical conversion); operation at a high current density maximizes the oxygen evolution side reaction, which is competitive with anodic oxidation by chemisorbed active oxygen (MO_{x+1} ; presumed to form through an oxygen transfer from adsorbed $\cdot\text{OH}$ to the

* Corresponding author at: Civil, Environmental, and Architectural Engineering, Korea University, Seoul 136-701, Republic of Korea.

E-mail address: lee39@korea.ac.kr (J. Lee).

lattice of the metal oxide anode (MO_x) [10,12]. On the other hand, a high O_2 evolution overpotential allows PbO_2 and doped SnO_2 electrodes to efficiently oxidize and mineralize a broad spectrum of persistent organics (i.e., electrochemical incineration) [10,13]. Boron-doped diamond (BDD) film as a high-oxidation-power anode, characterized by a wide potential window for water electrolysis (-1.35 to $+2.3$ V_{NHE} [14]), mechanical durability, and chemical inertness, also causes non-selective organic oxidation, thus treating recalcitrant wastewaters with high chemical oxygen demand (COD) [10,13,15,16]. In addition to direct electron abstraction, $\cdot\text{OH}$ -induced oxidation takes place on a BDD film due to its weak interaction with electrochemically formed active oxygen (postulated as the typical property of high O_2 overpotential anodes) [10]. Electrocatalytic activity of the conductive diamonds for pollutant oxidation [17] could be improved in the presence of transition metal ions (e.g., Fe^{2+}) or in combination with UV light [18,19].

Although salt-based electrolytes are generally supplied for reducing the electrical resistance between electrodes, electrochemical oxidation of electrolyte-derived free anions (e.g., Cl^- and SO_4^{2-}), which serve as the precursors of reactive oxidizing species, leads to secondary oxidative degradation pathways. For instance, the use of chloride-based electrolytes switched the reaction pathway electrochemically induced on an Sb-SnO₂ anode from $\cdot\text{OH}$ -induced oxidation to chlorination [20]. Electrochemical oxidation using a BDD anode in the presence of Cl^- resulted in a concomitant decrease in the COD and ammonium content of landfill leachates, because breakpoint chlorination by RCS occurred parallel to mineralization involving direct electron transfer and $\cdot\text{OH}$ -mediated oxidation [15]. The anodic oxidation of various organic pollutants by BDD electrodes markedly accelerated in aqueous SO_4^{2-} solutions rather than NO_3^- or ClO_4^- solutions; this was ascribed to the strong oxidizing capacity of sulfate radicals ($\text{SO}_4^{\cdot-}$) anodically formed from SO_4^{2-} [21]. Furthermore, peroxydisulfate (PDS) produced by $\text{SO}_4^{\cdot-}$ recombination could improve the oxidative degradation efficiency via two mechanisms: (i) additional $\text{SO}_4^{\cdot-}$ formation associated with cathodic PDS reduction [21] and (ii) non-radical persulfate activation mediated by BDD as a carbocatalyst [22]. Whereas metal-induced persulfate activation typically results from the one-electron oxidation of peroxide bond (accompanied by $\text{SO}_4^{\cdot-}$ formation), carbonaceous materials such as carbon nanotube, reduced graphene oxide, and thermally annealed nanodiamond decompose organics in the presence of persulfate via not only radical-induced route but also pathways involving no radical attack (e.g., singlet oxygenation, mediated electron transfer) [23,24].

The use of SO_4^{2-} as a proxy to Cl^- probably benefits BDD anodic water treatment, although earlier comparative studies [25,26] presented a superior performance of chloride-based electrolytes over sulfate-based ones. Firstly, $\text{SO}_4^{\cdot-}$ outperforms chloride-derived reactive intermediates (e.g., hypochlorous acid (HOCl)) in oxidatively treating recalcitrant organics. Secondly, as electrolysis on a BDD anode stoichiometrically oxidizes Cl^- into ClO_4^- with chlorine oxyanions at lower oxidation states (e.g., ClO_2^- and ClO_3^-) formed as intermediates [27], anodic SO_4^{2-} oxidation leads to the formation of the corresponding oxyanion PDS, which involves $\text{SO}_4^{\cdot-}$ recombination [28]. ClO_4^- , as an emerging contaminant, is extremely resistant to redox-induced transformation under ambient conditions [29], readily accumulating in the treatment system. In contrast, cathodic PDS reduction probably gives rise to a secondary route for $\text{SO}_4^{\cdot-}$ production [21,30], eventually returning SO_4^{2-} as the electrolyte. Finally, high-yield PDS generation inevitably takes place when applying BDD anodes for electrochemical organic oxidation in aqueous SO_4^{2-} solutions, which indicates that anodic water treatment would proceed parallel to the formation of the radical precursor (i.e., PDS). This could provide the opportunity for integration with post-activation processes utilizing heat [31] or UV light [32].

To explore the role of $\text{SO}_4^{\cdot-}$ as a secondary oxidizing species during electrochemical water treatment, we analyzed the electrochemical

oxidation on a BDD anode in the presence of NaCl , Na_2SO_4 , and NaClO_4 as supporting electrolytes, based on (i) multi-activity assessment using multiple organic substrates, (ii) electron paramagnetic resonance (EPR) spectral features, and (iii) repetition tests (without fresh electrolyte supply). We monitored the kinetic rate of 4-chlorophenol (4-CP) oxidation associated with PDS activation on diverse cathodic materials (e.g., Ti, Al, Cu, Sn, and stainless steel (SS)), which was correlated with the faradaic efficiency for sulfate evolution. As activation strategies for persulfate anodically generated from SO_4^{2-} , we examined ohmic heating (resulting from electrical resistance of water) and UV photolysis, which provided a collateral route for $\text{SO}_4^{\cdot-}$ production, in addition to anodic SO_4^{2-} oxidation and cathodic PDS activation.

2. Materials and methods

2.1. Reagents

All the chemicals were of reagent grade and were used as-received (see Text S1 in the Supplementary material). Ultrapure deionized water ($> 18 \text{ M}\Omega \text{ cm}$), produced with a Milli-Q water purification system, was used to prepare all the experimental solutions.

2.2. Electrochemical experimental set-up and operation

Electrochemical oxidation of organic pollutants was carried out in a magnetically stirred undivided reactor having a reaction volume of 160 mL, under constant current density conditions. An electrolysis current was applied using a direct current (DC) power supply (TPM-1010, Toyotech Co., Korea). The anodes and cathodes were rectangular plates with dimensions of 2 cm \times 5 cm (active geometric area: 10 cm^2), and were placed parallel, with a constant inter-electrode distance of 1 cm. In the electrolysis experiments, BDD (WESCO electrode) and Ti (Aldrich) typically served as the anode and cathode, respectively, and Na_2SO_4 at varying concentrations (0.25–1.5 M) was used as the supporting electrolyte in most cases. To confirm the contribution of cathodic PDS reduction to $\text{SO}_4^{\cdot-}$ formation, linear sweep voltammetry (LSV), chronopotentiometry (CP), and chronoamperometry (CA) measurements were performed using a three-electrode configuration cell connected to a computer-controlled potentiostat (Autolab POSTAT302N). The cell contained a BDD electrode, a saturated calomel electrode (SCE), and a metal plate (i.e., Ti, Al, Cu, Sn, or SS) as the working, reference, and counter electrodes, respectively. In the experiments to monitor SO_4^{2-} evolution during electrolysis in the presence of PDS as the catholyte, a Nafion117 membrane (cation-exchange membrane) was used to separate the anode compartment from the cathode compartment. LSV spectra were recorded with an applied scan rate of 50 mV/s, in the potential range of -2.0 to $+0.0$ V_{SCE} (the potential was scanned in the positive direction). CP at a constant current density of 300 mA/cm² was employed to monitor the time-dependent profiles of anode and cathode potentials during electrolytic oxidation (Figs. S1 and S2). To comparatively evaluate the PDS reduction capacity of metal-based cathodes (based on the faradaic efficiency for SO_4^{2-} production), CA analysis was conducted in a two-compartment cell, with variable potentials applied on cathodes in aqueous solutions containing PDS (at an initial concentration range of 0.03–0.3 M) and 1 M NaClO_4 (applied as a background electrolyte to maintain a constant conductivity).

2.3. Analytical methods

To monitor the rate of electrochemical oxidation of organic pollutants, including phenol, 4-CP, benzoic acid (BA), nitrobenzene (NB), cyanuric acid (CYA), perfluoroctanoate (PFOA), and perfluorooctanesulfonate (PFOS), 1 mL aliquots were withdrawn at constant time intervals from the cylindrical glass reactor, using a 1 mL syringe, filtered through a 0.45 μm PTFE filter (Whatman), transferred

into a 2 mL amber glass vial, and sealed for quantitative analysis of target substrates. The concentrations of all the organic compounds (except PFOA and PFOS) were measured using a high-performance liquid chromatography (HPLC; Agilent Infinity 1260) system equipped with a C-18 column (ZORBAX Eclipse XDB-C18) and a UV/vis detector (G1314F 1260VWD). The HPLC analysis was conducted with an eluent comprising a binary mixture of 0.1% (v/v) aqueous phosphoric acid and neat acetonitrile. PFOA and PFOS were quantified by Q Exactive™ Hybrid Quadrupole-Orbitrap™ mass spectrometry (Thermo Fisher Scientific Inc.) coupled with the rapid-separation liquid chromatography (RSLC; UltiMate 3000, Dionex Co.). The RSLC separation was performed on an Acclaim™ 120 C18 column (150 mm × 2.1 mm, 2.2 μm; Thermo Fisher Scientific Inc.) with a mobile phase consisting of 0.1% aqueous formic acid solution (80%) and methanol (20%). The heated electrospray ionization (ESI) source interface was operated in the negative ionization mode. Products formed during anodic 4-CP oxidation in the presence of Cl^- , SO_4^{2-} , and ClO_4^- as electrolytes were qualitatively analyzed using the Triple TOF 5600 mass spectrometry (AB Sciex) coupled with RSLC (equipped with an ESI interface in the negative ion mode). The separation was carried out on a U-VD Sphere PUR 100 C18-E column (100 mm × 2.1 mm, 1.8 μm; BGB Analytik AG) under gradient elution with acetonitrile-aqueous formic acid (0.1%) mixtures. SO_4^{2-} , ClO_3^- , and ClO_4^- were determined using an ion chromatograph (IC; Dionex DX120) equipped with a Dionex IonPac AS-14 and a conductivity detector. Peroxymonosulfate (PMS) and PDS were measured according to the colorimetric method proposed by Liang et al. [33], based on the iodine ($\lambda_{\text{max}} = 352$ nm) produced from the oxidation of iodide by PMS or PDS. For EPR detection of radical species such as $\text{SO}_4^{\cdot-}$ and $\cdot\text{OH}$, 5,5-dimethyl-pyrroline N-oxide (DMPO) was used as the spin-trapping agent. The EPR spectra were recorded during electrochemical oxidation on BDD anodes in aqueous electrolyte solutions, using a JES-TE 300 spectrometer (JEOL, Japan), under the following conditions: microwave power = 1 mW, microwave frequency = 9.418 GHz, center field = 3351 G, modulation width = 0.2 mT, and modulation frequency = 100 kHz.

2.4. Radiolysis experiment

To confirm the reactivity of the radical species (i.e., $\text{SO}_4^{\cdot-}$ and $\cdot\text{OH}$ presumed to be electrochemically produced on BDD anodes) toward select organics, including CYA, PFOA, and PFOS, we explored the possibility that the highly persistent organics could decay under γ -irradiation conditions. The γ -irradiation dosage levels were set high enough to cause the complete degradation of 1 mM phenol (Fig. S3). Organic oxidation induced by γ -irradiation (in the dose range of 5–50 kGy) was performed using a ^{60}Co source (Nordion Inc., Canada), in three experimental solutions: (i) air-equilibrated aqueous solution, (ii) N_2O -saturated aqueous solution, for selective formation of $\cdot\text{OH}$ ($\text{e}_{\text{aq}}^- + \text{N}_2\text{O} + \text{H}_2\text{O} \rightarrow \text{N}_2 + \cdot\text{OH} + \cdot\text{OH}$), and (ii) N_2 -saturated aqueous solution containing excess PDS (50 mM) and *t*-BuOH (0.2 M), for production of $\text{SO}_4^{\cdot-}$ as the predominant oxidant ($\text{e}_{\text{aq}}^- + \text{PDS} \rightarrow \text{SO}_4^{\cdot-} + \text{SO}_4^{2-}$, $k_1 = 1.2 \times 10^{10} \text{ M}^{-1} \text{ s}^{-1}$; and $\cdot\text{H} + \text{PDS} \rightarrow \text{SO}_4^{\cdot-} + \text{HSO}_4^-$, $k_2 = 2.5 \times 10^7 \text{ M}^{-1} \text{ s}^{-1}$) [34]. Butanol was added to scavenge $\cdot\text{OH}$ and $\cdot\text{H}$ ($(\text{CH}_3)_3\text{COH} + \cdot\text{OH} \rightarrow (\text{CH}_3)_2(\text{CH}_2)\text{COH} + \text{H}_2\text{O}$, $k_3 = 6.0 \times 10^8 \text{ M}^{-1} \text{ s}^{-1}$ [35]; and $(\text{CH}_3)_3\text{COH} + \cdot\text{H} \rightarrow (\text{CH}_3)_2(\text{CH}_2)\text{COH} + \text{H}_2$, $k_4 = 1.15 \times 10^6 \text{ M}^{-1} \text{ s}^{-1}$ [36]).

3. Results and discussion

3.1. Anodic oxidation of organics under varying electrolyte conditions

We monitored the electrochemical oxidation of multiple organic compounds, including phenol, 4-CP, BA, NB, and CYA, on BDD anodes, while varying the background electrolyte (i.e., NaCl , Na_2SO_4 , and NaClO_4) (Fig. 1). The degradation efficiency marginally changed, depending on the type of substrate, when ClO_4^- was used as the inert

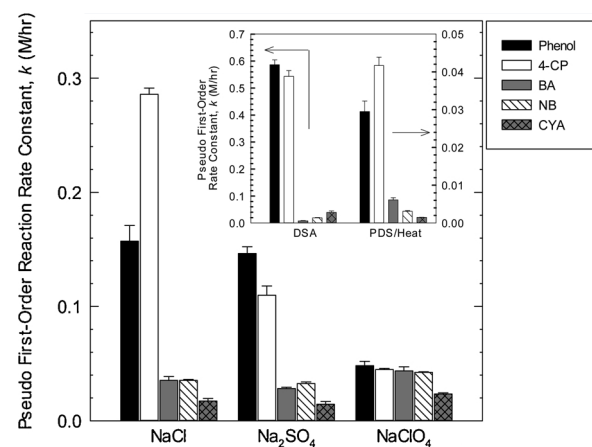


Fig. 1. Electrochemical oxidation of diverse organic compounds, including phenol, 4-chlorophenol (4-CP), benzoic acid (BA), nitrobenzene (NB), and cyanuric acid (CYA), on boron-doped diamond (BDD) anodes in aqueous solutions of NaCl , Na_2SO_4 , and NaClO_4 ($[\text{phenol}]_0 = [\text{4-CP}]_0 = [\text{NB}]_0 = [\text{CYA}]_0 = 10 \text{ mM}$; $[\text{BA}]_0 = 5 \text{ mM}$; current density = 300 mA/cm^2 ; $[\text{NaCl}]_0 = [\text{Na}_2\text{SO}_4]_0 = [\text{NaClO}_4]_0 = 1 \text{ M}$; $\text{pH}_i = 5.0$). Inset: oxidative degradation of organics during electrolysis on DSAs ($[\text{phenol}]_0 = [\text{4-CP}]_0 = [\text{BA}]_0 = [\text{NB}]_0 = [\text{CYA}]_0 = 1 \text{ mM}$; current density = 50 mA/cm^2 ; $[\text{NaCl}]_0 = 0.25 \text{ M}$; $\text{pH}_i = 5.0$) and by heat-activated peroxydisulfate ($[\text{phenol}]_0 = [\text{4-CP}]_0 = [\text{BA}]_0 = [\text{NB}]_0 = [\text{CYA}]_0 = 1 \text{ mM}$; $[\text{S}_2\text{O}_8^{2-}]_0 = 5 \text{ mM}$; temperature = 70°C ; $\text{pH}_i = 7.0$).

electrolyte, which suggests the role of $\cdot\text{OH}$ as the non-selective oxidant in anodic organic decomposition. The noticeable decay of CYA, which barely reacts with $\cdot\text{OH}$ [37], suggests the involvement of direct electron abstraction. In contrast, the electrolyte exchange from ClO_4^- to Cl^- or SO_4^{2-} , which act as the precursors of reactive oxidizing species, made the anodic oxidation performance substrate-specific; phenol and 4-CP oxidation proceeded at considerably faster rates than BA and NB oxidation, and CYA was more refractory to electro-oxidation than the other substrates. The higher susceptibility of phenolic compounds to anodic oxidation corroborated that electrolyte-derived reactive species could contribute to the overall electrochemical oxidation efficiency; aromatic compounds activated with electron-donating groups (i.e., phenol and 4-CP) are more prone to attack by selective oxidants than those possessing electron-withdrawing substituents (i.e., BA and NB). The selective nature allows the rate constants for reactions involving RCS and $\text{SO}_4^{\cdot-}$ to span a wide range [38,39]. For instance, the rate constants for $\text{Cl}_2^{\cdot-}$ -induced oxidation differ by two orders of magnitude depending on the type of substituent, with $k < 10^5\text{--}10^7 \text{ M}^{-1} \text{ s}^{-1}$ for aromatic compounds with electron-withdrawing groups versus $k = 10^7\text{--}10^9 \text{ M}^{-1} \text{ s}^{-1}$ for aromatic compounds with electron-donating groups [38]. The roles of anodically formed RCS and $\text{SO}_4^{\cdot-}$ were confirmed based on the substrate-dependent degradation efficiencies of two reference processes: electrochemical chlorination using DSA [11] and heat-induced persulfate activation [31] (inset of Fig. 1). The RCS electrochemically produced on DSA rapidly degraded phenol and 4-CP, whereas they decomposed NB very slowly, and did not oxidize BA at all. Preferential oxidation of phenol and 4-CP also proceeded during thermal PDS activation, but NB, with a low reactivity toward $\text{SO}_4^{\cdot-}$ ($k(\text{NB} + \text{SO}_4^{\cdot-}) < 10^6 \text{ M}^{-1} \text{ s}^{-1}$ [39]), underwent marginal decay. The kinetically retarded CYA degradation during electrolysis on BDD anodes in the presence of excess Cl^- and SO_4^{2-} seemed to result from the competition between CYA and the electrolyte for direct electron transfer.

BA was effectively oxidized during electrolysis on BDD anodes, irrespective of the electrolyte type (Fig. 2; note that electrochemical chlorination of BA was almost absent (inset of Fig. 1)). The observation that an organic substrate that is inert toward an electrolyte-derived oxidant (i.e., RCS) could be degraded on BDD anodes indicated that non-selective anodic oxidation took place parallel to indirect oxidation

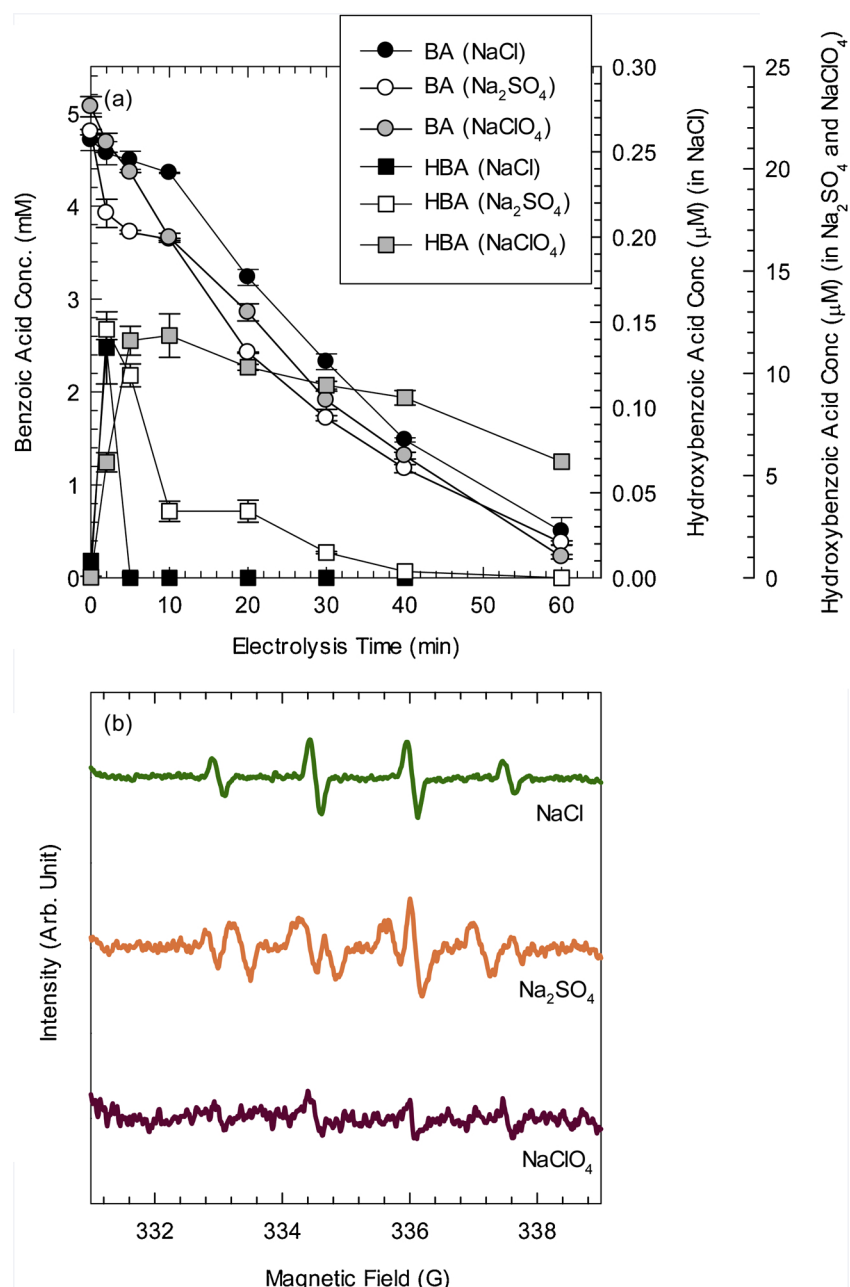


Fig. 2. (a) Electrochemical oxidation of benzoic acid (BA) and production of 4-hydroxybenzoic acid (4-HBA) on boron-doped diamond (BDD) anodes in aqueous solutions of NaCl, Na₂SO₄, and NaClO₄ ([BA]₀ = 5 mM; current density = 300 mA/cm²; [NaCl]₀ = [Na₂SO₄]₀ = [NaClO₄]₀ = 1 M; pH_i = 5.0). (b) Electron paramagnetic spectra obtained during electrolysis in aqueous solutions of NaCl, Na₂SO₄, and NaClO₄ ([DMPO]₀ = 10 mM; current density = 300 mA/cm²; [NaCl]₀ = [Na₂SO₄]₀ = [NaClO₄]₀ = 1 M; pH_i = 5.0).

by secondary oxidizing species. No difference in the BA degradation efficiency was found in aqueous Cl[−] and SO₄^{2−} solutions under identical conductivity conditions (Fig. S4). Regardless of the electrolyte used in the electrochemical system, 4-hydroxybenzoic acid (4-HBA) commonly formed, which, as an indication of radical-induced hydroxylation, suggested electrochemical ·OH production. Although the BA decay rate did not significantly vary depending on the electrolyte type, the period of time over which the concentration of the hydroxylated intermediate increased, reached the maximum, and fell to an undetectable level increased in the following order: Cl[−] < SO₄^{2−} < ClO₄[−] (Fig. 2a). This result seems compatible with the reactivity of the secondary oxidant toward 4-HBA; 4-HBA rapidly decomposed during electrochemical chlorination on the BDD anode, whereas 4-HBA oxidation was kinetically retarded in the aqueous

SO₄^{2−} solution (Fig. S5). This implies that electrolyte-derived oxidants contribute to the overall electrochemical oxidation process (oxidative treatment of not only the parent organic compound but also the intermediates). The formation of SO₄^{·−} due to the one-electron oxidation of SO₄^{2−} on the BDD anode was further evidenced based on the EPR spectra monitored under varying electrolyte conditions. Fig. 2b demonstrates that EPR spectral features assignable to SO₄^{·−} appeared during electrolytic oxidation in the aqueous SO₄^{2−} solution, whereas the EPR spectra observed for the aqueous Cl[−] and ClO₄[−] solutions corresponded to ·OH production.

The electrochemical oxidation of two organic contaminants, CYA and PFOA, as SO₄^{·−} probe compounds [40,41], was performed in aqueous solutions of different electrolytes (i.e., Cl[−], SO₄^{2−}, and ClO₄[−]) at initial concentrations adjusted for equivalent conductivity (Fig. 3).

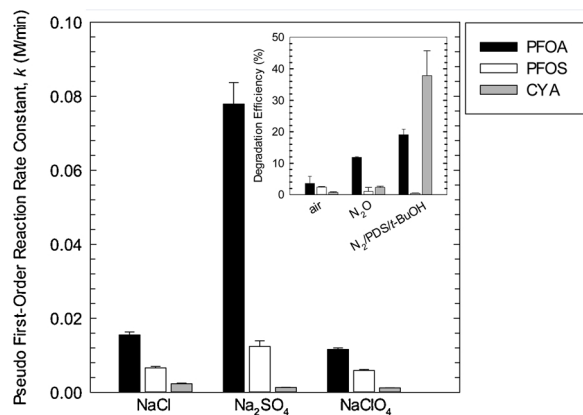


Fig. 3. Electrochemical oxidation of perfluoroctanoate (PFOA), perfluoroctanesulfonate (PFOS), and cyanuric acid (CYA) on boron-doped diamond (BDD) anodes utilizing Cl^- , SO_4^{2-} , and ClO_4^- as electrolytes under identical conductivity conditions ($[\text{PFOA}]_0 = [\text{PFOS}]_0 = 0.1 \text{ mM}$; $[\text{CYA}]_0 = 1 \text{ mM}$; $[\text{NaCl}]_0 = 0.53 \text{ M}$, $[\text{Na}_2\text{SO}_4]_0 = 0.4 \text{ M}$, $[\text{NaClO}_4]_0 = 0.55 \text{ M}$; conductivity = 53 mS/cm ; $\text{pH}_i = 5.0$). Inset: radiolytic degradation of PFOA, PFOS, and CYA in air-equilibrated and N_2O -saturated aqueous solutions and N_2 -saturated aqueous mixture consisting of peroxydisulfate and *tert*-butanol ($[\text{PFOA}]_0 = [\text{PFOS}]_0 = 0.1 \text{ mM}$; $[\text{CYA}]_0 = 1 \text{ mM}$; $[\text{S}_2\text{O}_8^{2-}]_0 = 50 \text{ mM}$; $[\text{t-BuOH}]_0 = 0.2 \text{ M}$; $\text{pH}_i = 5.0$).

The preferential oxidation of CYA and PFOA by $\text{SO}_4^{\cdot-}$ was confirmed, based on the experimental results, using the γ -radiolysis technique (inset of Fig. 3); PFOA and CYA more significantly decomposed when they were subjected to γ -radiolysis in the presence of excess PDS and *tert*-butanol (*t*-BuOH), which were added as a $\text{SO}_4^{\cdot-}$ precursor and a scavenger of $\cdot\text{OH}$ and H^{\cdot} , respectively (leading to selective $\text{SO}_4^{\cdot-}$ generation), than under N_2O -saturated conditions (causing selective $\cdot\text{OH}$ production). It is notable that almost no CYA was degraded in the N_2O -saturated solution. On the other hand, PFOS, which is highly resistant to oxidation by $\text{SO}_4^{\cdot-}$ [41], barely decomposed in N_2 -saturated aqueous mixtures of PDS and *t*-BuOH. The reactivity of $\text{SO}_4^{\cdot-}$, presented in the inset of Fig. 3, did not perfectly align with the substrate-specific performance of electrochemical oxidation using SO_4^{2-} as the electrolyte (Fig. 3). PFOA was electrochemically oxidized on the BDD anode at a much faster rate in the aqueous SO_4^{2-} solution than in the others ($k(\text{PFOA}) = 0.0779 \pm 0.0058 \text{ min}^{-1}$ for SO_4^{2-} , $k(\text{PFOA}) = 0.0155 \pm 0.0008 \text{ min}^{-1}$ for Cl^- , and $k(\text{PFOA}) = 0.0166 \pm 0.0004 \text{ min}^{-1}$ for ClO_4^-), which accords with the more effective PFOA treatment by $\text{SO}_4^{\cdot-}$ observed in the γ -radiolysis experiments. In contrast, the electrochemical degradation of CYA, which was highly susceptible to $\text{SO}_4^{\cdot-}$ -induced oxidation (inset of Fig. 3), was not markedly accelerated when SO_4^{2-} was used instead of Cl^- and ClO_4^- . This may have resulted from direct electron transfer, which would have substantially outperformed $\text{SO}_4^{\cdot-}$ -mediated oxidation in CYA degradation; excess SO_4^{2-} conditions may have favored direct electron abstraction from SO_4^{2-} rather than CYA, which would have retarded electrochemically induced direct organic oxidation involving no radical attack, while improving the $\text{SO}_4^{\cdot-}$ production yield. Electrochemical oxidation of PFOS, which negligibly reacted with $\text{SO}_4^{\cdot-}$ and $\cdot\text{OH}$ (inset of Fig. 3), was still noticeable with all the electrolytes used in this study (Fig. 3), and indicates a non-radical oxidation mechanism occurring on the BDD anodes [42].

To further evidence the role of electrolyte-derived oxidants in the electrochemical treatment of organic compounds, we performed the LC-MS analysis to identify the products formed during anodic 4-CP oxidation by varying the electrolyte type. Reaction pathways for anodic 4-CP treatment in the presence of different electrolytes were proposed in Fig. S6 based on the major products found in the mass chromatograms (Table S1 and Figs. S7–S9). Whereas hydroquinone (Product 3), maleic acid (or fumaric acid) (Product 4), and 4-chlorocatecol (Product

6) were commonly detected, regardless of electrolyte type, anodic oxidation processes operated in the presence of Cl^- and SO_4^{2-} yielded the product distributions that are clearly distinguishable. The use of Cl^- formed various secondary and tertiary (i.e., further oxidized) products, which include oxalic acid (Product 1), hydroxyquinol (Product 5), chloromaleic acid (or chlorofumaric acid) (Product 7), 5-chlorobenzene-1,2,4-triol (Product 8), and 3-chloro-4-hydroxyhexa-2,4-dienedioic acid (Product 10). Alternatively, chlorohydroxyphenyl sulfate (Product 11) and dichlorobiphenyl diol (Product 12), occurred distinctively when SO_4^{2-} was employed as an electrolyte. Detection of Products 11 and 12 supports the involvement of $\text{SO}_4^{\cdot-}$ in oxidative 4-CP transformation. Product 11 results from the addition of $\text{SO}_4^{\cdot-}$ to the aromatic ring [43], and Product 12 as a dimer forms through a series of reactions that reflect the reactivity of $\text{SO}_4^{\cdot-}$: (i) conversion of 4-CP into the corresponding phenol radical cation through one-electron abstraction by $\text{SO}_4^{\cdot-}$, (ii) rearrangement to phenoxyl radical, and (iii) radical recombination (i.e., dimerization) [44]. Overall, product distributions (Table S1) and proposed reaction routes (Fig. S6) confirm that the pathway for anodic organic oxidation could be modified hinging on the type of electrolyte.

3.2. Effects of current density and electrolyte concentration

We monitored the electrochemical oxidation of phenol and BA on BDD anodes in aqueous solutions of Cl^- , SO_4^{2-} , and ClO_4^- , while varying the electrolyte concentration and current density (Figs. S10 and S11). Regardless of the electrolyte type, the efficiency for electrochemical organic oxidation was gradually promoted by an increase in the current density and electrolyte concentration, but the extent of improvement in treatment performance varied depending on the substrate type. The enhancing effects became more pronounced when phenol was electrochemically oxidized in aqueous Cl^- solutions; the phenol oxidation efficiency reached the maximum level at a relatively low Cl^- concentration and current density range (Figs. S10a and S11a). This was likely due to a more preferential oxidation of Cl^- ($E^0(\text{HOCl}/\text{Cl}^-) = 1.49 \text{ V}_{\text{NHE}}$ [45]; $E^0(\text{SO}_4^{\cdot-}/\text{SO}_4^{2-}) = 2.5\text{--}3.1 \text{ V}_{\text{NHE}}$ [46]), followed by the production of RCS that were capable of rapid phenol degradation. On the other hand, the use of SO_4^{2-} and ClO_4^- as electrolytes favored electrochemical BA degradation over a wide current density range (Fig. S11b), which could be attributed to the high susceptibility of BA to $\text{SO}_4^{\cdot-}$ -induced oxidation and direct electron abstraction (BA persists in the electrochemical chlorination process (inset of Fig. 1)). BA decay in the aqueous ClO_4^- solution was faster than that in the aqueous Cl^- solution, under varying electrolyte concentration, which was likely due to the competition between BA and Cl^- for direct electron abstraction. It is worth noting that NaCl and NaClO_4 exhibited almost the same conductivity when they were added at identical concentrations (caption of Fig. 3).

3.3. Repeated anodic oxidation of phenol

The use of Cl^- as the electrolyte allowed effective RCS evolution on the BDD anode, which caused a rapid degradation of organic compounds that were highly vulnerable to chlorination (Fig. 1). In particular, a breakpoint chlorination electrochemically induced on the BDD anode enabled the transformation of ammonia into nitrogen, with minimal formation of nitrate [15], which was in marked contrast to the stoichiometric conversion of ammonia into nitrate when SO_4^{2-} was used as the supporting electrolyte (Fig. S12). Due to the high oxidation power of the BDD anode, the electrochemical oxidation of organics performed in the presence excess Cl^- was accompanied by the successive conversion of Cl^- into ClO_4^- [27]. A high yield of ClO_4^- on the BDD anode gives rise to environmental concern, owing to the (i) adverse biological effect of ClO_4^- and (ii) strong resistance of ClO_4^- to redox-mediated treatment processes [29]. Considering that the persulfate produced via anodic oxidation of SO_4^{2-} can be readily transformed

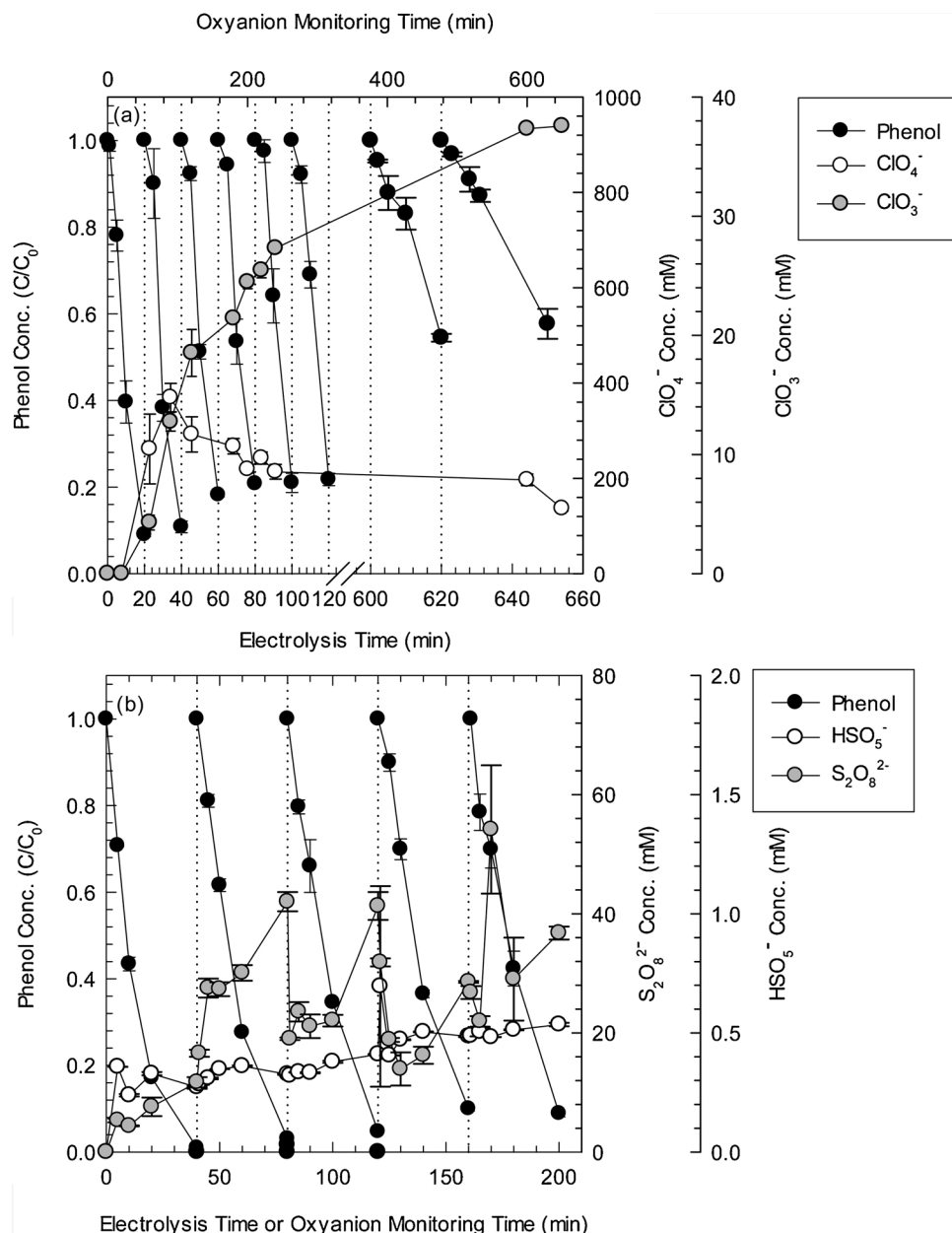


Fig. 4. Repeated electrochemical oxidation of phenol on boron-doped diamond (BDD) anodes, and evolution of electrolyte-derived oxyanions in aqueous solutions of (a) NaCl and (b) Na₂SO₄ ([phenol]₀ = 10 mM; current density = 300 mA/cm²; [NaCl]₀ = [Na₂SO₄]₀ = 1 M; pH_i = 5.0).

back into SO₄²⁻ in several ways (e.g., cathodic reduction [22] and photolysis [32]), the choice of SO₄²⁻ as the electrolyte would mitigate the secondary contamination with electrolyte-derived oxyanions, and enable an improvement in the treatment performance associated with persulfate activation (discussed later).

Oxidative conversion of electrolytes into the corresponding oxyanions inevitably occurs on BDD anodes, simultaneously with the electrochemical incineration of organics. Owing to the extremely high persistence of ClO₄⁻, the irreversible multi-electron oxidation of Cl⁻ to ClO₄⁻ continued in the presence of an applied current, and therefore, the repeated electrolytic oxidation on the BDD electrode in the chloride electrolyte caused a significant electrolyte replacement (from Cl⁻ to ClO₄⁻) (Fig. 4a). The electrolyte exchange (which decreases the concentration of Cl⁻ as a precursor of RCS) probably reduced the electrocatalytic activity of the BDD anode for organic oxidation; the phenol degradation efficiency gradually diminished as the electrochemical oxidation was repeatedly performed, and the rate of phenol oxidation

decreased by half when the conversion of Cl⁻ to ClO₄⁻ was ca. 90% (Fig. 4a). On the other hand, the electrochemical redox reaction in the aqueous sulfate electrolyte led to an interconversion between SO₄²⁻ and persulfate, which prevented a rapid electrolyte replacement (from SO₄²⁻ to PDS or PMS); the efficiency for conversion of Cl⁻ to ClO₄⁻ was ca. 13 times higher than that for the transformation of SO₄²⁻ into PDS (Fig. 4a and b). The moderate electrolyte exchange maintained the performance of SO₄²⁻-induced phenol oxidation (Fig. 4b), but would render SO₄²⁻ to continually compete with organics for anodic oxidation (it is notable that ClO₄⁻ was not involved anymore in electrolytic redox reactions once the irreversible anodic oxidation of Cl⁻ to ClO₄⁻ was complete).

3.4. Cathodic activation of anodically formed persulfate

To explore the possibility of cathodic activation of PDS (confirmed to be anodically produced, as shown in Fig. 4b), LSV, CP, and CA

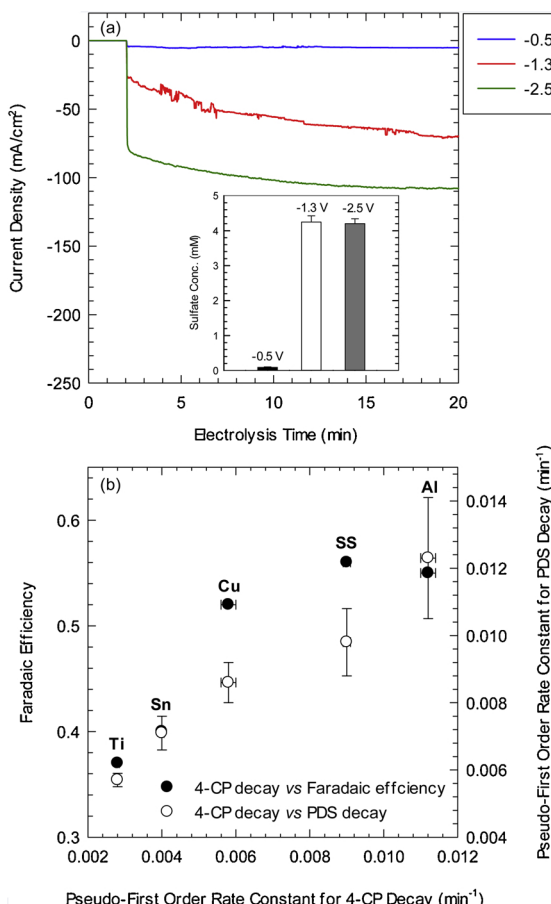


Fig. 5. (a) Chronoamperometric response obtained in the presence of peroxydisulfate (PDS), with varying potential applied to Ti cathode ($[S_2O_8^{2-}]_0 = 30 \text{ mM}$; $[\text{NaClO}_4]_0 = 1 \text{ M}$; $pH_i = 5.0$) and (b) correlation between faradaic efficiency for sulfate formation (or PDS decay rate) and 4-chlorophenol (4-CP) oxidation rate measured with diverse cathode materials ($[4\text{-CP}]_0 = 1 \text{ mM}$; current density = 10 mA/cm^2 ; $[S_2O_8^{2-}]_0 = 30 \text{ mM}$; $pH_i = 5.0$). Inset: sulfate formation from PDS at various potentials.

measurements were conducted with diverse cathode materials (i.e., Al, SS, Cu, Sn, and Ti) in the presence of PDS as the electrolyte. In the LSV curves (Fig. S13), the cathodic current gradually increased with an increase in the PDS concentration, regardless of the cathode type, which indicates the capability of all the tested cathodes for the reductive conversion of PDS to SO_4^{2-} (or SO_4^{1-}). The CA response observed on the Ti cathode in the potential range of -0.5 to $-2.5 \text{ V}_{\text{SCE}}$ also confirms the reductive PDS transformation; a noticeable reduction current was produced as more negative potential was applied to the cathode (Fig. 5a), accompanied by SO_4^{2-} evolution (inset of Fig. 5a). It is noteworthy that current generation and SO_4^{2-} formation occurred at cathode potentials more negative than *ca.* $-1.2 \text{ V}_{\text{SCE}}$, which correspond to the potential at which the extent of increase in cathodic current became more pronounced in the LSV curves (Fig. S13). In contrast, no detectable amount of Cl^- formed during electrolytic ClO_4^- reduction at substantially negative potentials (i.e., -2.5 and $-3.5 \text{ V}_{\text{SCE}}$) (inset of Fig. S14), and the reduction current (probably produced by proton or oxygen reduction) barely increased when the applied potential was shifted to a more negative value (from -2.5 to $-3.5 \text{ V}_{\text{SCE}}$) (Fig. S14).

We also elucidated the correlation between the rate of 4-CP oxidation, rate of PDS reduction, and faradaic efficiency for SO_4^{2-} formation (calculated according to Text S2; based on CA curves recorded using diverse cathodes (Fig. S15)) measured during electrolysis in aqueous PDS solutions with diverse cathodes (Fig. 5b). The rate of electrolytic 4-CP degradation (presumed to have been partially caused by cathodic

PDS activation) increased in the following order: Al > SS > Cu > Sn > Ti. The dependence of the 4-CP oxidation efficiency on the type of cathode was in perfect accordance with the rate of PDS decay monitored while varying the cathode material; a faster PDS reduction led to a more effective 4-CP decomposition. The faradaic efficiency for the formation of SO_4^{2-} as a PDS reduction product changed depending on the cathode type, and also correlated to a certain extent with the 4-CP degradation efficiency measured during electrolysis in the presence of PDS. The use of cathodes (e.g., SS and Cu) that exhibited a relatively high faradaic efficiency caused a more rapid 4-CP degradation, whereas the lowest faradaic and 4-CP oxidation efficiencies were observed on Ti. The cathodic conversion of PDS into SO_4^{2-} , which probably involves the formation of SO_4^{1-} as an intermediate, was linked with organic oxidation mediated by cathodically formed SO_4^{1-} ; this result implies the contribution of cathodic PDS reduction to SO_4^{1-} yield. Furthermore, the EPR spectra obtained in aqueous PDS solutions further confirmed that SO_4^{1-} could be cathodically generated from PDS (Fig. S16).

3.5. Persulfate activation by ohmic heating and UV photolysis

The electrolysis of an aqueous SO_4^{2-} solution using a BDD anode leads to the formation of SO_4^{1-} , which contributes, as a reactive intermediate, to organic oxidation, and undergoes recombination to produce persulfate [28]. PDS, which steadily accumulated as electrolysis in the presence of SO_4^{2-} progressed, is exploitable as a radical precursor, considering that the energy transfer processes convert PDS into SO_4^{1-} through homolytic peroxide bond dissociation [31,32,41]. Over the course of electrochemical organic oxidation, the current that flows through salt-containing water causes heat generation due to the electrical resistance of water (i.e., ohmic heating [47]). Two events, persulfate formation and resistive heating, which unavoidably occur during electrochemical water treatment using BDD anodes, could provide a non-electrochemical route for SO_4^{1-} production, based on the earlier findings [31,41] that thermal PDS activation involving SO_4^{1-} formation is achievable at elevated temperatures (e.g., $40\text{--}90^\circ\text{C}$). To explore the possibility of heat-induced PDS activation, we monitored the efficiency of the electrochemical transformation of SO_4^{2-} into persulfate, while changing the initial concentration of the sulfate-based electrolyte (Fig. 6a). The concentration of electrochemically generated persulfate increased in proportion with the concentration of SO_4^{2-} initially added. While PMS formed at relatively low levels, the PDS formation yield was *ca.* 6–36% when aqueous SO_4^{2-} solutions in concentrations of $0.25\text{--}1.5 \text{ M}$ were electrolyzed on BDD anodes for 40 min (Fig. 6a). The extent of the temperature rise also depended on the initial electrolyte concentration (inversely proportional), and the temperature level ($\sim 40\text{--}60^\circ\text{C}$) observed after aqueous SO_4^{2-} solutions were subjected to 40 min ohmic heating was sufficiently high for initiating thermal PDS activation (Fig. 6a). Over a wide range of SO_4^{2-} concentration, the concomitant PDS formation and heat generation during electrolysis on BDD anodes allowed significant 4-CP degradation to continue, even in the absence of an applied current (Fig. 6a); with a relatively high level of SO_4^{2-} as the electrolyte (1 or 1.5 M), 0.5 mM 4-CP completely decomposed over a 2 h reaction, after the current was switched off. On the other hand, PDS at the maximum concentration that we could observe over the course of electrolysis (i.e., 0.5 M) could not directly decompose 4-CP at room temperature (Fig. S17). No detectable 4-CP degradation occurred (after pre-electrolysis for 40 min) when Cl^- was alternatively used as the electrolyte (Fig. S18).

Since both PMS and PDS photochemically dissociate to form radicals (i.e., $\cdot\text{OH}$ and SO_4^{1-}) [32,48], UV irradiation would probably enhance electrochemical organic oxidation on the BDD anode by activating anodically formed persulfate (mainly PDS). UV photolysis subsequent to electrolysis using the BDD anode caused significant BA oxidation, owing to photochemical activation of persulfate, which gradually accumulated as a result of electrochemical SO_4^{2-} oxidation (it is notable that BA hardly decomposed during direct UV photolysis)

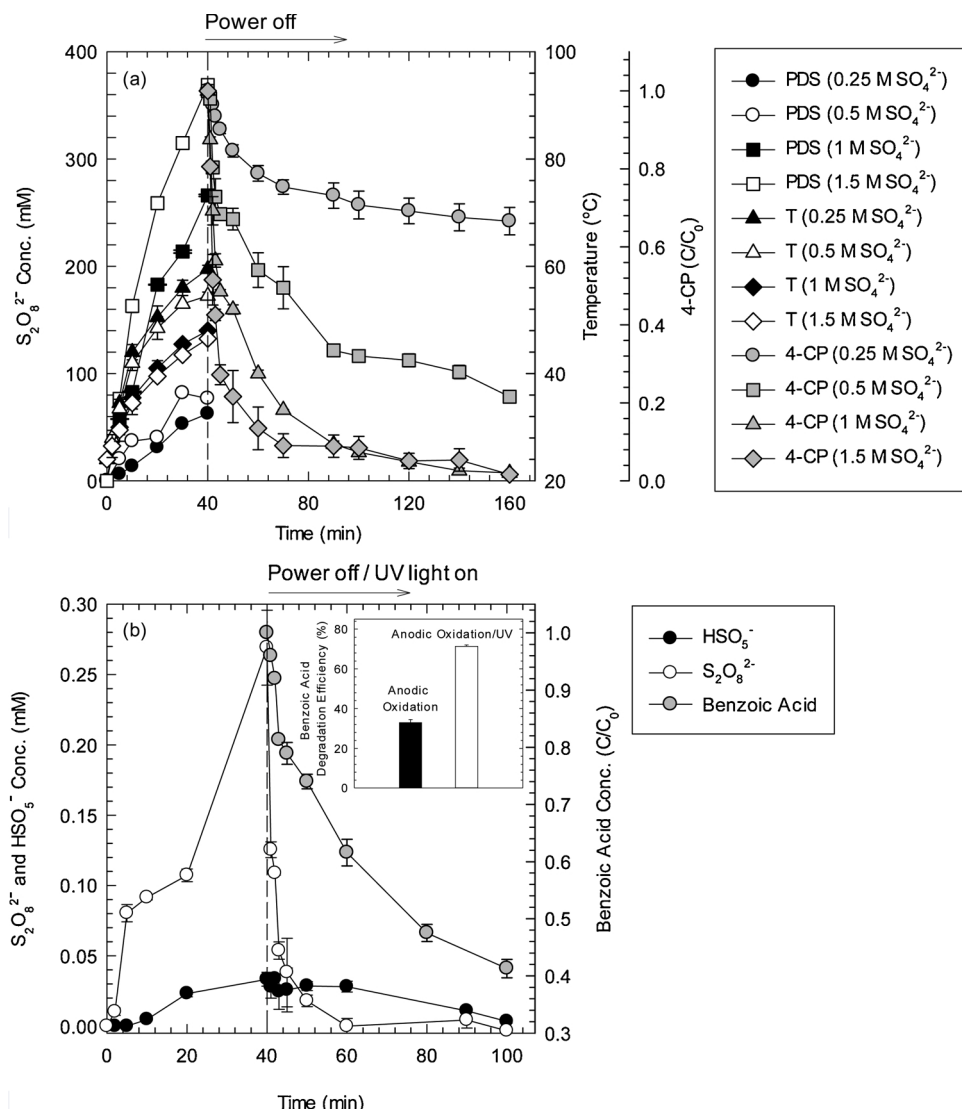


Fig. 6. (a) Changes in peroxydisulfate (PDS) concentration and temperature during pre-electrolysis on boron-doped diamond (BDD) anodes in the presence of Na_2SO_4 , and activation of anodically formed PDS by ohmic heating (leading to 4-chlorophenol (4-CP) oxidation without applied current) ($[4-CP]_0 = 0.5$ mM; current density = 300 mA/cm²; $pH_i = 5.0$), and (b) anodic production of PDS and peroxymonosulfate (PMS) followed by UV photolysis (leading to benzoic acid (BA) degradation in the absence of applied current) ($[BA]_0 = 0.1$ mM; current density = 10 mA/cm²; $[Na_2SO_4]_0 = 30$ mM; $pH_i = 5.0$). Inset: comparison of anodic oxidation alone and anodic oxidation combined with UV photolysis, in terms of BA degradation efficiency.

(Fig. 6b). The combination of UV photolysis and electrolysis also accelerated the oxidative degradation of BA ($k(BA) = 0.0072 \pm 0.0006$ min⁻¹ for electrolysis, versus $k(BA) = 0.0217 \pm 0.0007$ min⁻¹ for photo-assisted electrolysis), which was associated with the photo-activation of electrochemically generated persulfate (inset of Fig. 6b). The photochemical activation of persulfate, which inevitably forms during electrochemical organic oxidation in the presence of SO_4^{2-} , prevents possible secondary contamination due to persulfate release, and enables the recycle of SO_4^{2-} , in addition to providing additional treatment performance.

3.6. Technical feasibility analysis

The extent of organic mineralization was determined based on the total organic carbon (TOC) level measured after 60 min electrolytic oxidation of 4-CP in aqueous Cl^- , SO_4^{2-} , and ClO_4^- solutions (Fig. S19a). The efficiency for TOC removal increased in the following order: ClO_4^- (70%) < SO_4^{2-} (77%) < Cl^- (81%). The extent of TOC loss was ranked in the same order when phenol was alternatively used as a model substrate (Fig. S19b): ClO_4^- (54%) < SO_4^{2-} (68%) < Cl^- (82%). The results seem to be aligned with the product distribution (Table S1); intermediates were further transformed into secondary and tertiary products (e.g., hydroxyquinol, chloromaleic acid, oxalic acid) when electrolysis was performed in the presence of Cl^- . We compared

three anodic processes utilizing Cl^- , SO_4^{2-} , and ClO_4^- as electrolytes in terms of energy cost when applying them for oxidative 4-CP treatment. Provided that the conductivity of the experimental solutions barely differs depending on the type of electrolyte, anodic processes operated in aqueous Cl^- and SO_4^{2-} solutions show the comparable specific energy consumption (SEC) value (defined as the amount of electric energy required to remove a unit mass of TOC; computed according to equation (1)), with $SEC = 514.96$ kWh kg_{TOC}⁻¹ for Cl^- and $SEC = 519.33$ kWh kg_{TOC}⁻¹ for SO_4^{2-} . However, the alternative choice of ClO_4^- led to *ca.* 16% increase in SEC (604.59 kWh kg_{TOC}⁻¹).

$$SEC = \frac{V_c \times I \times t}{(TOC_0(\text{or organic}_0) - TOC_f(\text{or organic}_f)) \times V} \quad (1)$$

where V_c is the voltage measured during the electrolysis, I is the applied electric current, t is the reaction time, TOC_0 (or $organic_0$) and TOC_f (or $organic_f$) are the initial and final TOC values (or the initial mass and final mass of target substrate), respectively, and V is the volume of the experimental solution. Further, there is a need to take anodically produced persulfate into account in energy cost analysis. With the ratio of H_2O_2 cost to electricity cost (the average ratio was reported to be *ca.* 10.81 kWh kg⁻¹ H_2O_2 for the five local regions surveyed) [49], the amount of persulfate generated during 60 min electrolysis on BDD anode in the presence of SO_4^{2-} (i.e., 4.6 g) could be converted into electricity. Since the price of PDS is about half the price of H_2O_2 [50], it

would correspond to *ca.* 25 Wh (close to the electric energy consumed to anodically remove 77% of the initial TOC in the presence of SO_4^{2-} i.e., *ca.* 23 Wh) (Fig. S19a).

To assess the technical practicability of integrating electrolysis and photolysis, we also compared electrolysis alone and combined electrolysis-photolysis in terms of 4-CP treatment efficiency under varying light intensity condition. Fig. S20 confirmed that the combination of electrolysis with photolysis could improve oxidative treatment performance: increasing 4-CP degradation efficiency by *ca.* 20% with electric energy for UV irradiation (2.81 Wh) consumed additionally. However, based on the SEC value (the amount of electric energy required to remove unit mass of 4-CP), the combined system seems not to be superior to the single system, with $\text{SEC} = 86.94 \text{ kWh kg}_{4\text{-CP}}^{-1}$ for the combined system versus $\text{SEC} = 66.05 \text{ kWh kg}_{4\text{-CP}}^{-1}$ for the single system. Nevertheless, UV photolysis deserves consideration as a viable technical option for not only additionally promoting treatment performance but also preventing undesirable persulfate discharge (leading to secondary contamination) and regenerating sulfate as an electrolyte (without need of extra sulfate supply). Note that cathodic PDS reduction alone could not afford to completely reduce anodically generated PDS based on the observed gradual PDS accumulation with increasing catalytic cycle (Fig. 4b). In particular, since electrochemical reactions occur locally in the inter-electrode regions, scaling up the electrochemical system would more severely limit the efficiency for cathodic persulfate activation. Accordingly, UV photolysis is a feasible complement to cathodic reduction now that it readily activates persulfate released to the bulk phase without being subjected to activation on cathode. Further, in that there is much margin for efficiency improvement through the optimization of reactor configuration, lamp arrangement pattern, spacing between light sources or between a light source and a reactor, light source type, and reaction parameters, the separate in-depth study is required to more accurately access the combined system in terms of energy efficiency. Apart from the cost-effectiveness based on the SEC, the combined electrolysis-photolysis would enable the on-site oxidative water treatment requiring no or minimal chemical reagents, thus reducing the costs resulting from persulfate synthesis, transport, and storage.

4. Conclusions

In an effort to clarify the possible technical benefits of SO_4^{2-} as an electrolyte, we delved into the roles of the reactive intermediates (SO_4^{1-} and persulfate) generated from SO_4^{2-} , in electrochemical oxidative degradation of organics on BDD anodes. The involvement of SO_4^{1-} as a secondary oxidant was confirmed based on (i) substrate-specificity that accorded with the reactivity of SO_4^{1-} (produced from PDS activation by heat or γ -radiolysis) and (ii) EPR spectral features assignable to SO_4^{1-} formation. Some earlier studies [21,51] showed that the use of SO_4^{2-} as the electrolyte markedly accelerated the electrochemical oxidation of all the organic substrates tested on BDD anodes, owing to the powerful oxidizing capacity of anodically formed SO_4^{1-} . However, the enhancing effect was not pronounced in this study; the electrolyte replacement from Cl^- to SO_4^{2-} did not improve the efficiency for anodic oxidation of organic compounds (except PFOA). The potential advantage of using SO_4^{2-} instead of Cl^- lies in the reversible conversion of SO_4^{2-} to PDS, which is accompanied by SO_4^{1-} generation. The extreme resistance of ClO_4^- resulting from anodic Cl^- oxidation toward redox reactions caused the electrolyte-derived oxyanion to gradually accumulate in the electrochemical water treatment process, which led to (i) unwanted discharge of ClO_4^- as an emerging recalcitrant contaminant and (ii) reduction in RCS production efficiency associated with the depletion of Cl^- as a precursor of RCS. On the other hand, as demonstrated in Figs. 5 and 6a, b, PDS, which inevitably forms during anodic organic oxidation in the presence of SO_4^{2-} , was activated to produce SO_4^{1-} , by cathodic reduction, ohmic heating (exploiting the inherent electrical resistance of water), and

combination with UV photolysis (in sequence or simultaneously), being eventually transformed back to SO_4^{2-} . This allows for repeated utilization of SO_4^{2-} , minimal formation of PDS, which may cause secondary contamination, and an improved performance in oxidative organic decomposition. Similar to in-situ cathodic H_2O_2 production (from dissolved oxygen) followed by UV photolysis (recently suggested to be suitable for decentralized water treatment) [52], activation processes subsequent to anodic persulfate formation (from SO_4^{2-} as the electrolyte) can be explored as point-of-source water treatment strategies that require no external supply of chemical additives. In addition, considering that extremely high sulfate concentration (*ca.* 0.13–0.5 M) occurs in acid mine drainage [53,54] or wastewaters discharged from coal-fired power plants [55], electrochemical process utilizing BDD anode would achieve the concomitant treatment of organic contaminants from sulfate-laden wastewaters and production of persulfate that is convertible to SO_4^{1-} in various manners: cathodic reduction, ohmic heating, and UV photolysis.

Acknowledgements

This study was supported by the National Research Foundation of Korea grant funded by the Korean government (MSIT) (NRF-2018R1A4A1022194), the National Research Foundation of Korea grant funded by the Ministry of Science, ICT, and Future Planning (No. 2016M3A7B4909318), and Korea Ministry of Environment as "The SEM projects 2018" (RE201805163).

Appendix A. Supplementary data

Supplementary material related to this article can be found, in the online version, at doi:<https://doi.org/10.1016/j.apcatb.2019.04.060>.

References

- [1] B.C. Hedges, E.L. Cates, J.H. Kim, Challenges and prospects of advanced oxidation water treatment processes using catalytic nanomaterials, *Nat. Nanotechnol.* 13 (2018) 642–650.
- [2] M.A. Oturan, J.J. Aaron, Advanced oxidation processes in water/wastewater treatment: principles and applications: a review, *Crit. Rev. Environ. Sci. Technol.* 44 (2014) 2577–2641.
- [3] J.A. Zazo, J.A. Casas, A.F. Mohedano, M.A. Gilarranz, J.J. Rodriguez, Chemical pathway and kinetics of phenol oxidation by Fenton's reagent, *Environ. Sci. Technol.* 39 (2005) 9295–9302.
- [4] I.A. Katsoyannis, S. Canonica, U. von Gunten, Efficiency and energy requirements for the transformation of organic micropollutants by ozone, $\text{O}_3/\text{H}_2\text{O}_2$ and $\text{UV}/\text{H}_2\text{O}_2$, *Water Res.* 45 (2011) 3811–3822.
- [5] M.R. Hoffmann, S.T. Martin, W.Y. Choi, D.W. Bahnemann, Environmental applications of semiconductor photocatalysis, *Chem. Rev.* 95 (1995) 69–96.
- [6] C.Y. Zhou, C. Lai, D.L. Huang, G.M. Zeng, C. Zhang, M. Cheng, L. Hu, J. Wan, W.P. Xiong, M. Wen, X.F. Wen, L. Qin, Highly porous carbon nitride by supramolecular preassembly of monomers for photocatalytic removal of sulfamethazine under visible light driven, *Appl. Catal. B: Environ.* 220 (2018) 202–210.
- [7] C.Y. Zhou, C. Lai, C. Zhang, G.M. Zeng, D.L. Huang, M. Cheng, L. Hu, W.P. Xiong, M. Chen, J.J. Wang, Y. Yang, L.B. Jiang, Semiconductor/boron nitride composites: synthesis, properties, and photocatalysis applications, *Appl. Catal. B: Environ.* 238 (2018) 6–18.
- [8] C.A. Martinez-Huitl, S. Ferro, Electrochemical oxidation of organic pollutants for the wastewater treatment: direct and indirect processes, *Chem. Soc. Rev.* 35 (2006) 1324–1340.
- [9] J. Radjenovic, D.L. Sedlak, Challenges and opportunities for electrochemical processes as next-generation technologies for the treatment of contaminated water, *Environ. Sci. Technol.* 49 (2015) 11292–11302.
- [10] M. Panizza, G. Cerisola, Direct and mediated anodic oxidation of organic pollutants, *Chem. Rev.* 109 (2009) 6541–6569.
- [11] Y.U. Shin, H.Y. Yoo, S. Kim, K.M. Chung, Y.G. Park, K.H. Hwang, S.W. Hong, H. Park, K. Cho, J. Lee, Sequential combination of electro-Fenton and electrochemical chlorination processes for the treatment of anaerobically-digested food wastewater, *Environ. Sci. Technol.* 51 (2017) 10700–10710.
- [12] C. Cominellis, Electrocatalysis in the electrochemical conversion/combustion of organic pollutants for waste water treatment, *Electrochim. Acta* 39 (1994) 1857–1862.
- [13] C.A. Martinez-Huitl, M.A. Quiroz, C. Cominellis, S. Ferro, A. De Battisti, Electrochemical incineration of chloranilic acid using Ti/IrO_2 , Pb/PbO_2 and Si/BDD electrodes, *Electrochim. Acta* 50 (2004) 949–956.
- [14] L. Pujol, D. Evrard, K. Groenen-Serrano, M. Freyssinier, A. Ruffien-Cizsak, P. Gros,

Electrochemical sensors and devices for heavy metals assay in water: the French groups' contribution, *Front. Chem.* 2 (2014).

[15] A. Anglada, A. Urtiaga, I. Ortiz, Pilot scale performance of the electro-oxidation of landfill leachate at boron-doped diamond anodes, *Environ. Sci. Technol.* 43 (2009) 2035–2040.

[16] A. Anglada, A. Urtiaga, I. Ortiz, D. Mantzavinos, E. Diamadopoulos, Boron-doped diamond anodic treatment of landfill leachate: evaluation of operating variables and formation of oxidation by-products, *Water Res.* 45 (2011) 828–838.

[17] E. Guinea, F. Centellas, E. Brillas, P. Canizares, C. Saez, M.A. Rodrigo, Electrocatalytic properties of diamond in the oxidation of a persistent pollutant, *Appl. Catal. B: Environ.* 89 (2009) 645–650.

[18] E. Guinea, F. Centellas, J.A. Garrido, R.M. Rodriguez, C. Arias, P.L. Cabot, E. Brillas, Solar photoassisted anodic oxidation of carboxylic acids in presence of Fe^{3+} using a boron-doped diamond electrode, *Appl. Catal. B: Environ.* 89 (2009) 459–468.

[19] I. Sires, F. Centellas, J.A. Garrido, R.M. Rodriguez, C. Arias, P.L. Cabot, E. Brillas, Mineralization of clofibrate acid by electrochemical advanced oxidation processes using a boron-doped diamond anode and Fe^{2+} and UVA light as catalysts, *Appl. Catal. B: Environ.* 72 (2007) 373–381.

[20] Y.Y. Ahn, S.Y. Yang, C. Choi, W. Choi, S. Kim, H. Park, Electrocatalytic activities of $Sb-SnO_2$ and $Bi-TiO_2$ anodes for water treatment: effects of electrocatalyst composition and electrolyte, *Catal. Today* 282 (2017) 57–64.

[21] A. Farhat, J. Keller, S. Tait, J. Radjenovic, Removal of persistent organic contaminants by electrochemically activated sulfate, *Environ. Sci. Technol.* 49 (2015) 14326–14333.

[22] H.R. Song, L.X. Yan, J. Jiang, J. Ma, Z.X. Zhang, J.M. Zhang, P.X. Liu, T. Yang, Electrochemical activation of persulfates at BDD anode: radical or nonradical oxidation? *Water Res.* 128 (2018) 393–401.

[23] X.G. Duan, H.Q. Sun, Z.P. Shao, S.B. Wang, Nonradical reactions in environmental remediation processes: uncertainty and challenges, *Appl. Catal. B: Environ.* 224 (2018) 973–982.

[24] X.G. Duan, H.Q. Sun, S.B. Wang, Metal-free carbocatalysis in advanced oxidation reactions, *Acc. Chem. Res.* 51 (2018) 678–687.

[25] S. Kim, S.K. Choi, B.Y. Yoon, S.K. Lim, H. Park, Effects of electrolyte on the electrocatalytic activities of RuO_2/Ti and $Sb-SnO_2/Ti$ anodes for water treatment, *Appl. Catal. B: Environ.* 97 (2010) 135–141.

[26] C.Y. Zhang, Z.F. Zhang, Z.Z. He, D.G. Fu, New insights into the relationship between anode material, supporting electrolyte and applied current density in anodic oxidation processes, *Electrochim. Acta* 229 (2017) 55–64.

[27] O. Azizi, D. Hubler, G. Schrader, J. Farrell, B.P. Chaplin, Mechanism of perchlorate formation on boron-doped diamond film anodes, *Environ. Sci. Technol.* 45 (2011) 10582–10590.

[28] J. Davis, J.C. Baygents, J. Farrell, Understanding persulfate production at boron doped diamond film anodes, *Electrochim. Acta* 150 (2014) 68–74.

[29] K.D. Hurley, J.R. Shapley, Efficient heterogeneous catalytic reduction of perchlorate in water, *Environ. Sci. Technol.* 41 (2007) 2044–2049.

[30] W.S. Chen, Y.C. Jhou, C.P. Huang, Mineralization of dinitrotoluenes in industrial wastewater by electro-activated persulfate oxidation, *Chem. Eng. J.* 252 (2014) 166–172.

[31] C.Q. Tan, N.Y. Gao, Y. Deng, N. An, J. Deng, Heat-activated persulfate oxidation of diuron in water, *Chem. Eng. J.* 203 (2012) 294–300.

[32] Y.Q. Gao, N.Y. Gao, Y. Deng, Y.Q. Yang, Y. Ma, Ultraviolet (UV) light-activated persulfate oxidation of sulfamethazine in water, *Chem. Eng. J.* 195 (2012) 248–253.

[33] C.J. Liang, C.F. Huang, N. Mohanty, R.M. Kurakalva, A rapid spectrophotometric determination of persulfate anion in ISCO, *Chemosphere* 73 (2008) 1540–1543.

[34] J. Paul, D.B. Naik, Y.K. Bhardwaj, L. Varshney, Studies on oxidative radiolysis of ibuprofen in presence of potassium persulfate, *Radiat. Phys. Chem.* 100 (2014) 38–44.

[35] G.V. Buxton, C.L. Greenstock, W.P. Helman, A.B. Ross, Critical review of rate constants for reactions of hydrated electrons, hydrogen-atoms and hydroxyl radicals ($\cdot OH/\cdot O^-$) in aqueous solution, *J. Phys. Chem. Ref. Data* 17 (1988) 513–886.

[36] L. Wojnarovits, E. Takacs, K. Dajka, S.S. Emmi, M. Russo, M. D'Angelantonio, Re-evaluation of the rate constant for the H atom reaction with *tert*-butanol in aqueous solution, *Radiat. Phys. Chem.* 69 (2004) 217–219.

[37] G.Y. Liu, Recalcitrance of cyanuric acid to oxidative degradation by OH radical: theoretical investigation, *RSC Adv.* 4 (2014) 37359–37364.

[38] K. Zhang, K.M. Parker, Halogen radical oxidants in natural and engineered aquatic systems, *Environ. Sci. Technol.* 52 (2018) 9579–9594.

[39] P. Neta, V. Madhavan, H. Zemel, R.W. Fessenden, Rate constants and mechanism of reaction of SO_4^{2-} with aromatic compounds, *J. Am. Chem. Soc.* 99 (1977) 163–164.

[40] P. Manoj, R. Varghese, V.M. Manoj, C.T. Aravindakumar, Reaction of sulphate radical anion ($SO_4^{\cdot-}$) with cyanuric acid: a potential reaction for its degradation? *Chem. Lett.* (2002) 74–75.

[41] T.A. Bruton, D.L. Sedlak, Treatment of perfluoroalkyl acids by heat-activated persulfate under conditions representative of in situ chemical oxidation, *Chemosphere* 206 (2018) 457–464.

[42] K.E. Carter, J. Farrell, Oxidative destruction of perfluorooctane sulfonate using boron-doped diamond film electrodes, *Environ. Sci. Technol.* 42 (2008) 6111–6115.

[43] G. Merga, C.T. Aravindakumar, B.S.M. Rao, H. Mohan, J.P. Mittal, Pulse radiolysis study of the reactions of SO_4^{2-} with some substituted benzenes in aqueous solution, *J. Chem. Soc. Faraday Trans.* 90 (1994) 597–604.

[44] Y.F. Ji, Y.Y. Shi, Y. Yang, P.Z. Yang, L. Wang, J.H. Lu, J.H. Li, L. Zhou, C. Ferronato, J.M. Chovelon, Rethinking sulfate radical-based oxidation of nitrophenols: formation of toxic polynitrophenols, nitrated biphenyls and diphenyl ethers, *J. Hazard. Mater.* 361 (2019) 152–161.

[45] A. Copeland, D.A. Lytle, Measuring the oxidation-reduction potential of important oxidants in drinking water, *J. Am. Water Works Assoc.* 106 (2014) E10–E20.

[46] P. Neta, R.E. Huie, A.B. Ross, Rate constants for reactions of inorganic radicals in aqueous solution, *J. Phys. Chem. Ref. Data* 17 (1988) 1027–1284.

[47] C.P. Samaranayake, S.K. Sastry, Electrode and pH effects on electrochemical reactions during ohmic heating, *J. Electroanal. Chem.* 577 (2005) 125–135.

[48] M. Mahdi-Ahmed, S. Chiron, Ciprofloxacin oxidation by UV-C activated peroxymonosulfate in wastewater, *J. Hazard. Mater.* 265 (2014) 41–46.

[49] E.J. Rosenfeldt, K.G. Linden, S. Canonica, U. von Gunten, Comparison of the efficiency of OH radical formation during ozonation and the advanced oxidation processes O_3/H_2O_2 and UV/H_2O_2 , *Water Res.* 42 (2008) 2836–2838.

[50] S. Waclawek, H.V. Lutze, K. Grubel, V.V.T. Padil, M. Cernik, D.D. Dionysiou, Chemistry of persulfates in water and wastewater treatment: a review, *Chem. Eng. J.* 330 (2017) 44–62.

[51] J. Radjenovic, M. Petrovic, Sulfate-mediated electrooxidation of X-ray contrast media on boron doped diamond anode, *Water Res.* 94 (2016) 128–135.

[52] J.M. Barazesh, T. Hennebel, J.T. Jasper, D.L. Sedlak, Modular advanced oxidation process enabled by cathodic hydrogen peroxide production, *Environ. Sci. Technol.* 49 (2015) 7391–7399.

[53] W.A.M. Fernando, I.M.S.K. Ilankoon, T.H. Syed, M. Yellishetty, Challenges and opportunities in the removal of sulphate ions in contaminated mine water: a review, *Miner. Eng.* 117 (2018) 74–90.

[54] S. Klimkova, M. Cernik, L. Lacinova, J. Filip, D. Jancik, R. Zboril, Zero-valent iron nanoparticles in treatment of acid mine water from in situ uranium leaching, *Chemosphere* 82 (2011) 1178–1184.

[55] S. Lee, Y. Kim, S. Hong, Treatment of industrial wastewater produced by desulfurization process in a coal-fired power plant via FO-MD hybrid process, *Chemosphere* 210 (2018) 44–51.